Crystal structures of Ca^{2+}–calmodulin bound to Na_V C-terminal regions suggest role for EF-hand domain in binding and inactivation

Bernd R. Gardill[a], Ricardo E. Rivera-Acevedo[a,1], Ching-Chieh Tung[a], and Filip Van Petegem[a,2]

[a]Department of Biochemistry and Molecular Biology, Life Sciences Institute, The University of British Columbia, Vancouver, BC, Canada V6T 1Z3

Edited by Richard W. Aldrich, The University of Texas at Austin, Austin, TX, and approved April 16, 2019 (received for review October 29, 2018)

Voltage-gated sodium (Na_V) and calcium channels (Ca_V) form targets for calmodulin (CaM), which affects channel inactivation properties. A major interaction site for CaM resides in the C-terminal (CT) region, consisting of an IQ domain downstream of an EF-hand domain. We present a crystal structure of fully Ca^{2+}-occupied CaM, bound to the CT of $Na_V1.5$. The structure shows that the C-terminal lobe binds to a site ∼90° rotated relative to a previous site reported for an apoCaM complex with the $Na_V1.5$ CT and for ternary complexes containing fibroblast growth factor homologous factors (FHF). We show that the binding of FHFs forces the EF-hand domain in a conformation that does not allow binding of the Ca^{2+}-occupied C-lobe of CaM. These observations highlight the central role of the EF-hand domain in modulating the binding mode of CaM. The binding sites for Ca^{2+}-free and Ca^{2+}-occupied CaM contain targets for mutations linked to long-QT syndrome, a type of inherited arrhythmia. The related $Na_V1.4$ channel has been shown to undergo Ca^{2+}-dependent inactivation (CDI) akin to Ca_Vs. We present a crystal structure of Ca^{2+}/CaM bound to the $Na_V1.4$ IQ domain, which shows a binding mode that would clash with the EF-hand domain. We postulate the relative reorientation of the EF-hand domain and the IQ domain as a possible conformational switch that underlies CDI.

sodium channel | inactivation | cardiac arrhythmia | long-QT syndrome | calcium-dependent inactivation

Voltage-gated sodium channels (Na_Vs) can rapidly depolarize an excitable cell by allowing the influx of extracellular Na^+ ions (1). Mammalian Na_Vs typically assemble from different subunits. The principal component is the $Na_V\alpha$ subunit, which forms a 24-transmembrane (TM) helix membrane protein. These are organized in four homologous repeats (I–IV), connected by long linkers (I–II linker, II–III linker, and III–IV linker) that are intrinsically disordered. In mammalian species, nine isoforms exist ($Na_V1.1$–1.9), which differ in expression profile, pharmacology, and electrophysiological properties. The primary isoform expressed in cardiac muscle is $Na_V1.5$. In contrast, the auxiliary $Na_V\beta$ subunit encodes a smaller protein with an extracellular Ig-like domain, a single TM helix, and a short cytosolic intracellular tail (2).

Recent advances in cryo-EM have allowed reconstructions of $Na_V1.4$ from electric eels (3) and humans (4) and an Na_v from the American cockroach (5). In addition, high-resolution crystal structures have been reported for the Ig domains of mammalian $Na_V\beta2$, β3, and β4 (6–9). Despite these advances, the bulk of the cytosolic region appeared invisible in the cryo-EM reconstructions, suggesting inherent flexibility relative to the TM region. With the exception of the cockroach Na_V structure, no interpretable density was present downstream of the last TM segment.

The C-terminal region (CT) of the $Na_V\alpha$ subunits encode an EF-hand–like domain, immediately downstream of the last TM segment (10–12). EF-hand domains are frequently observed to bind Ca^{2+}, but thus far all available crystal structures have been unable to reveal Ca^{2+} density even at high Ca^{2+} concentrations (13). In the cryo-EM structure of the cockroach Na_V, the EF-hand–like domain is found to interact with the III–IV linker (5). NMR experiments suggest that this interaction also occurs in mammalian Na_Vs, and that it regulates the degree of channel inactivation (14). The EF-hand–like domain is followed by two α-helices, one which latches on to the domain termed the "pre-IQ helix" and a second one containing an IQ motif. The IQ motif forms a binding site for both Ca^{2+}-free and Ca^{2+}-occupied calmodulin (CaM), a ubiquitous Ca^{2+} sensor that endows many proteins with Ca^{2+}-dependent regulation.

Several roles have been postulated for CaM binding to Na_Vs and unfortunately there is disagreement on the precise functions (15). Multiple groups have reported a depolarizing shift in the steady-state inactivation curves at elevated cytosolic Ca^{2+} levels (micromolar range) (12, 16–20). However, this was not recapitulated in an experiment with Ca^{2+} uncaging, and in the case of one particular isoform, $Na_V1.4$, Ca^{2+}/CaM was found to promote inactivation in a manner similar to voltage-gated calcium channels (Ca_V) (21). In several Ca_V isoforms, CaM causes a robust acceleration of current inactivation for several isoforms (CDI, Ca^{2+}-dependent inactivation) (22–24). Since these Ca_V isoforms also contain a CT encoding EF-hands and an IQ domain, the way CaM interacts with and modulates these channels may be very similar. Indeed, it was found that chimeric $Ca_V1.3$ channels with the $Na_V1.4$ CT also display CDI, further highlighting the similarities

Significance

Calmodulin (CaM) is a Ca^{2+}-sensing protein that endows several voltage-gated sodium (Na_V) and calcium (Ca_V) channels with Ca^{2+}-dependent inactivation (CDI). Although this phenomenon has been known to exist for decades, the exact mechanism remains at large. Several high-resolution structures have captured complexes between Ca^{2+}/CaM and Na_V or Ca_V C-terminal IQ domains, but structures are scarce for a larger $(Ca^{2+})_4$/CaM complex that also includes the upstream EF-hand domain, a domain that is critical for CDI. We show crystal structures of the C-terminal domain of the cardiac Nav1.5 and the IQ domain of $Na_V1.4$, two Na_Vs that are differentially regulated by CaM. The results uncover a role for the EF-hand domain in dictating binding of CaM and suggest a conformational switch in CDI.

Author contributions: B.R.G., R.E.R.-A., and F.V.P. designed research; B.R.G., R.E.R.-A., C.-C.T., and F.V.P. performed research; B.R.G., R.E.R.-A., C.-C.T., and F.V.P. analyzed data; and B.R.G. and F.V.P. wrote the paper.

The authors declare no conflict of interest.

This article is a PNAS Direct Submission.

Data deposition: Crystal structures have been deposited in the Protein Data Bank, www.wwpdb.org (PDB ID codes 6MUD and 6MUE).

[1]Present address: Department of Anesthesiology, Pharmacology, and Therapeutics, The University of British Columbia, Vancouver, BC, Canada V6T 1Z3.

[2]To whom correspondence should be addressed. Email: filip.vanpetegem@gmail.com.

This article contains supporting information online at www.pnas.org/lookup/suppl/doi:10.1073/pnas.1818618116/-/DCSupplemental.

Published online May 9, 2019.

between both channels (21). Despite these parallels, there is also divergence, as Na_V CT fragments bind Ca^{2+}-free CaM stronger than Ca^{2+}/CaM, opposite to most Ca_V1 and Ca_V2 channels. In addition, Na_V CT fragments can bind FHF proteins, whereas Ca_V CTs do not (13, 25, 26). CaM has also been reported to interact with the III–IV linker in $Na_V1.5$ (16, 27), but so far this has not yet been described for Ca_Vs.

There is thus great interest in trying to understand how CaM interacts with the CT of both Na_V and Ca_V channels, in both Ca^{2+}-free (apoCaM) and Ca^{2+}-occupied (Ca^{2+}/CaM) forms. So far, the IQ domain has remained invisible in all Na_V and Ca_V cryo-EM reconstructions, and all structural insights have thus come from crystallographic and NMR studies. For Ca_V channels, all high-resolution studies only contain the isolated IQ domain with or without a pre-IQ helix, thus not showing the role of the EF-hand region (28–32). For Na_V channels, however, crystal structures containing the longer CT, encompassing EF-hands and IQ domain, are available. One report was for a ternary complex between CaM, the $Na_V1.5$ CT, and FGF13, a fibroblast growth factor homologous factor (FHF) (25). Mg^{2+} was bound in the Ca^{2+} binding sites, and thus the conformation of the lobes is that of an apoCaM. We therefore refer to this structure as an apoCaM complex. The structure showed the apoC-lobe interacting with the N-terminal portion of the IQ domain, with the apoN-lobe not being involved in the interaction. Another report also captured the $Na_V1.5$ CT in complex with apoCaM, but this time in the absence of an FHF protein (33). This shows the apoC-lobe to interact with the IQ domain at the same site as in the presence of the FHF protein. Additional interactions were also observed between the apoN-lobe and the $Na_V1.5$ EF-hand domain. The authors also noted a different relative orientation of the EF-hand domain to the IQ domain depending on the presence of an FHF (33). An NMR study of the $Na_V1.5$ IQ domain in complex with apoCaM also showed that the interaction is driven by the C-lobe, with a flexible N-lobe relative to the IQ domain (11). Another NMR study also supports an apoCaM interaction with the IQ domain that is driven by the C-lobe (34). In addition, ternary complexes were solved for the $Na_V1.5$ or $Na_V1.2$ CT in complex with CaM and an FHF in saturating Ca^{2+} concentrations (13). Although reported as a Ca^{2+}/CaM complex of the Na_V CT, the C-lobe did not display the open conformation observed for Ca^{2+}/CaM, and this structure is in disagreement with NMR studies of isolated IQ domains in complex with Ca^{2+}/CaM lobes (35, 36). Therefore, a structure of Ca^{2+}/CaM bound to the CT of either an Na_V or Ca_V, containing both IQ domain and EF-hands, has not yet been reported.

Here, we report a crystal structure of Ca^{2+}/CaM bound to the $Na_V1.5$ CT. Although a previous structure was previously reported as a Ca^{2+}/CaM complex (13), we show here that this is a misinterpretation and that the C-lobe was in the apo form. Our data show that the presence of the EF-hand is crucial in dictating the exact binding mode of CaM on the IQ domain, and that altering the conformation of the EF-hand domain through auxiliary proteins like FHFs can prevent Ca^{2+}/CaM from binding to the IQ domain. We also investigate the differences between Ca^{2+}/CaM binding to different Na_V isoforms, which hint at a possible mechanism for CDI.

Results

Crystal Structure of Ca^{2+}/CaM Bound to the $Na_V1.5$ CT. We solved a 2.7-Å structure of a complex between Ca^{2+}/CaM and the human $Na_V1.5$ CT, residues 1786–1922 (Fig. 1). All CaM EF-hand residues were well-resolved with clear density for Ca^{2+} ions, and unambiguous density for the IQ domain (*SI Appendix*, Fig. S1). A portion of the $Na_V1.5$ CT, encoded by residues 1879–1886, displayed poor density. This is in contrast to other structures [Protein Data Bank (PDB) ID codes 4DCK and 4OVN], where this loop is involved in interactions with other proteins or crystal contacts. The relative orientation of the EF-hand domain to the IQ domain is similar to a previously reported structure of apoCaM in complex with the $Na_V1.5$ CT (33), with a salt bridge formed between Asp1846, located in the EF-hand domain, and Arg1898 at the N-terminal end of the IQ domain. This EF-hand position is rotated ∼180° in comparison with ternary complexes of a Na_VCT with CaM and FHF proteins (13, 25). All interactions of Ca^{2+}/CaM with the $Na_V1.5$ CT are formed by the Ca^{2+}/C-lobe, which engages the N-terminal portion of the IQ domain. The Ca^{2+}/N-lobe does not engage any $Na_V1.5$ residue in the structure, but this does not preclude a possible downstream binding site for the Ca^{2+}/N-lobe, not part of the crystallized construct.

The interface between the $Na_V1.5$ IQ domain and the Ca^{2+}/C-lobe in this complex (PDB ID code 6MUD) is unusual (Fig. 1*B*). In many Ca^{2+}/CaM complexes, hydrophobic residues contribute to the binding of the target. In the $Na_V1.5$ IQ domain, only one

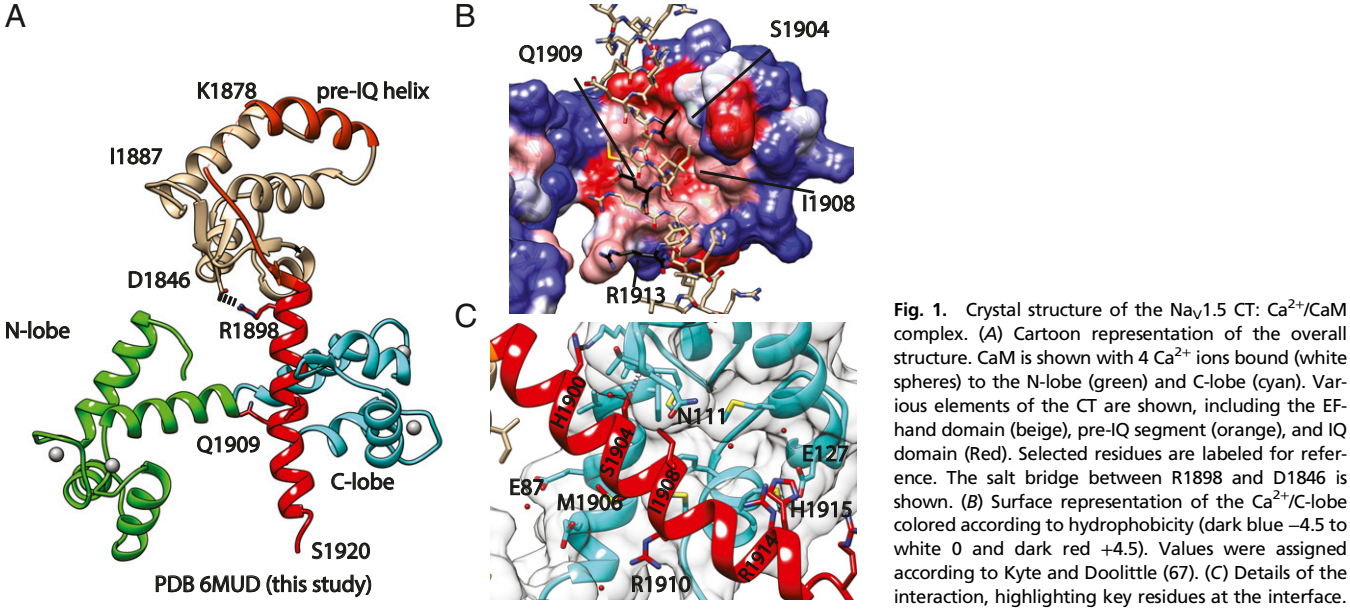

Fig. 1. Crystal structure of the $Na_V1.5$ CT: Ca^{2+}/CaM complex. (*A*) Cartoon representation of the overall structure. CaM is shown with 4 Ca^{2+} ions bound (white spheres) to the N-lobe (green) and C-lobe (cyan). Various elements of the CT are shown, including the EF-hand domain (beige), pre-IQ segment (orange), and IQ domain (Red). Selected residues are labeled for reference. The salt bridge between R1898 and D1846 is shown. (*B*) Surface representation of the Ca^{2+}/C-lobe colored according to hydrophobicity (dark blue −4.5 to white 0 and dark red +4.5). Values were assigned according to Kyte and Doolittle (67). (*C*) Details of the interaction, highlighting key residues at the interface.

Phe is present, which lies on the opposite side from the C-lobe interface. Instead, the side chains of Val1903 and Val1907 make hydrophobic contacts with the C-lobe, whereas the pocket lined by C-lobe residues Met124, Phe141, and Met144 is only occupied by a water molecule. A water molecule has been found at a similar location in a high-resolution structure of Ca^{2+}/CaM without peptide bound (PDB ID code 1EXR) (37). Other interactions of note involve IQ domain residues His1900, Ser1904, Met1906, Ile1908, and Arg1914 (Fig. 1*C*). Given the absence of typical aromatic anchors, the interaction is relatively weak. Indeed, isothermal titration calorimetry (ITC) experiments titrating C-lobe into the IQ domain under saturating Ca^{2+} concentrations showed an affinity (K_d) of ∼6 μM (16).

These interactions are very different from the ones observed for apoCaM with $Na_V1.5$ CT (PDB ID code 4OVN), as the C-lobe is rotated around the IQ domain by ∼90° (Fig. 2). ApoCaM engages $Na_V1.5$ residue Phe1912, whereas Ca^{2+}/CaM does not. This likely underlies the large difference in affinity, as the apoCaM affinity for the $Na_V1.5$ CT is an order of magnitude higher than Ca^{2+}/CaM (16).

It has been suggested that the Ca^{2+}/C-lobe also interacts with the EF-hand domain in Ca_Vs (38). In our structure, we observe a van der Waals interaction between EF-hand domain residue Ile1833 and C-lobe residue Glu87, suggesting only a modest contribution to the binding affinity. Investigation of the electrostatic surface potential suggests no major effect of electrostatics on the interaction between the Ca^{2+}/C-lobe and EF-hand domain (*SI Appendix*, Fig. S2). In agreement with this, comparison of ITC data for binding of Ca^{2+}/C-lobe to the $Na_V1.5$ CT (residues 1773–1924) showed an affinity not significantly different from the affinity to the individual IQ domain (16).

The Role of the EF-Hand Domain in Dictating the Binding Mode of CaM. Previously, Wang et al. (13) published a crystal structure that was proposed to represent a complex between Ca^{2+}/CaM and the CT of $Na_V1.2$ and $Na_V1.5$. However, as noted by Hovey et al. (36), a closer inspection of these structures (PDB ID codes 4JPZ and 4JQ0) shows that the C-lobes display a semiopen conformation such as observed in complexes of apoCaM with myosin V (39). Indeed, a direct superposition of the C-lobe with the one in our current structure shows a very different conformation (Fig. 2*A*). Instead, the C-lobe conformation by Wang et al. (13) closely resembles the conformation found in a structure of apoCaM in complex with the $Na_V1.5$ CT. In contrast, the N-lobe in the complex by Wang et al. (13) displays the typical open conformation for a Ca^{2+}-occupied lobe (Fig. 2 *B* and *C*). Irregularities in the difference density maps, as well as unexpected geometries for Ca^{2+}-chelating residues in EF-hands 3 and 4 for these structure (PDB ID codes 4JPZ and 4JQ0), were previously also reported by Hovey et al. (36). We further refer to this structure containing a Ca^{2+}/N-lobe and apoC-lobe conformation as a mixed CaM.

How could saturating levels of Ca^{2+} (2 to 100 mM) used by Wang et al. (13) result in a mixed CaM? Fig. 2*D* shows a direct comparison of the Ca^{2+}/CaM and mixed CaM complexes with the $Na_V1.5$ CT. The view is based on superposing the IQ domain, showing the relative positions of the individual lobes using the IQ domain as reference. Importantly, the Ca^{2+}/C-lobe binding

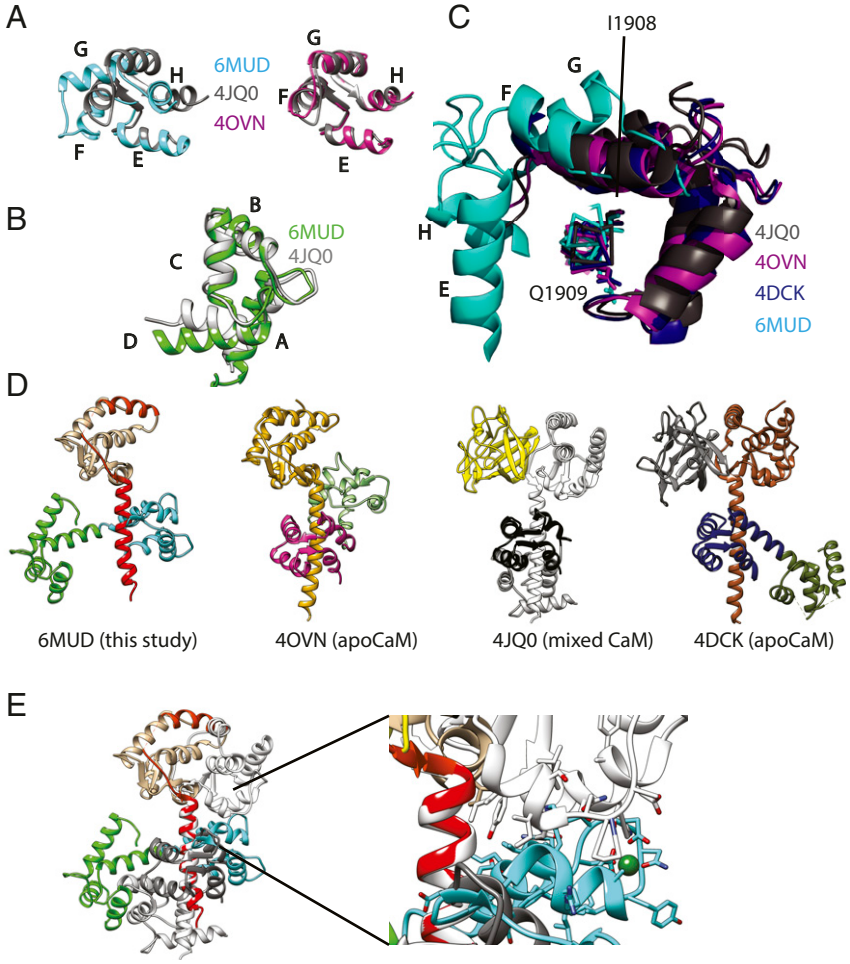

Fig. 2. Structural comparison. (*A*) Comparisons of the C-lobe conformation from this study (PDB ID code 6MUD, blue), a C-lobe from a previously proposed Na_VCT:Ca^{2+}/CaM complex (PDB ID code 4JQ0, gray), and an apoC-lobe (PDB ID code 4OVN, magenta), which shows that the previously proposed Ca^{2+}/C-lobe from a Na_V CT complex (13) is an apoC-lobe, not a Ca^{2+}/C-lobe. The letters in *A*–*C* correspond to the CaM helices. (*B*) Comparisons of the N-lobe from this study (green) with the N-lobe from PDB ID code 4JQ0 (gray), confirming that the latter represents a Ca^{2+}-occupied N-lobe. (*C*) Superpositions showing the relative C-lobe positions found in this study (6MUD, cyan) and three other previous CaM complex with the $Na_V1.5$ CT. (*D*) Side-by-side comparison of the current structure (PDB ID code 6MUD) and three other CaM complexes, including two apo-CaM complexes (PDB ID codes 4OVN and 4DCK) and one previously proposed Ca^{2+}/CaM complex, which is a mixed CaM (PDB ID code 4JQ0). The structures are shown in the exact same view, based on a superposition of the sixth helix immediately after the EF-hand domain. (*E*) Superposition of the Ca^{2+}/CaM (PDB ID code 6MUD) and mixed CaM (PDB ID code 4JQ0) complexes with $Na_V1.5$CT, based on the sixth helix containing the IQ domain, using the same colors as in *D*. This shows that the Ca^{2+}/C-lobe (cyan) from the $Na_V1.5$ CT: Ca^{2+}/CaM structure would clash with the $Na_V1.5$ EF-hand domain in the mixed CaM complex (PDB ID code 4JQ0). Therefore, binding of the Ca^{2+}/C-lobe to the IQ domain is prevented by the FHF, which utilizes reorientation of the EF-hand domain as a mechanism to prevent Ca^{2+}/C-lobe binding.

site is on the opposite face of the IQ helix compared with the apoC-lobe site. The direct comparison reveals a crucial role for the $Na_V1.5$ EF-hand domain, which adopts a very different orientation relative to the IQ domain. The EF-hand domain, as observed in the mixed-CaM complex, would clash with the Ca^{2+}/C-lobe in our structure (Fig. 2*E*).

One crucial difference in the conditions used in this report and by Wang et al. (13) is the presence of an FHF in the latter complex. Gabelli et al. (33) previously noted a different relative position of EF-hand domain to IQ domain comparing apoCaM complexes in the presence and absence of FHF. Fig. 3 shows four complexes, two in high Ca^{2+} and two in nominally Ca^{2+}-free conditions, with either an FHF present or absent. This shows that the relative conformation of EF-hand domain to IQ domain is nearly identical in the absence of FHF, regardless of whether Ca^{2+} is present or absent. Conversely, the two complexes containing FHF both show a similar relative EF-hand to IQ domain conformation, very different from the complexes without FHF. This shows that the relative orientation is dictated by the presence or absence of FHF, and not by Ca^{2+}.

In our Ca^{2+}/CaM:$Na_V1.5$ CT complex, the relative orientation of EF-hand to IQ domain is stabilized by a salt bridge between Arg1898, at the N terminus of the IQ domain, and Asp1846 in the EF-hand domain. Additional stabilizing interactions are formed via Thr1894 and Thr1895, and by stacking with Ile1836 (*SI Appendix*, Fig. S3). Similar interactions are also observed in the apoCaM:$Na_V1.5$ IQ complex (PDB ID code 4OVN) in all five molecules of the asymmetric unit. In the complexes with FHF, however, Arg1898 is directly sequestered, forming cation-π interactions with a Tyr residue of FGF13, an additional hydrogen bond to the backbone of Tyr98 and van der Waals interactions with Leu142 in FGF13. These observations thus directly explain the inability of a Ca^{2+}/C-lobe to bind to the IQ domain of $Na_V1.5$ in the presence of FHF: Since the latter disrupts the interaction between IQ domain and EF-hand domain, the EF-hand domain is now forced into a position that would clash with the Ca^{2+}/C-lobe. As a result, the C-lobe is forced to bind to the IQ domain in a Ca^{2+}-free conformation. These observations highlight the role of the EF-hand domain as a molecular switch, dictating the mode in which CaM can associate with the IQ domain. This observation likely underlies the functional effects of FHF proteins on Na_V inactivation (13, 25).

Contribution of Both Ca^{2+}/CaM Lobes to the Interaction. Although the structure by Wang et al. (13) displays an apoC-lobe conformation, the N-lobe was clearly bound to Ca^{2+} and was in turn found to interact with the IQ domain. This opens the possibility that fully saturated Ca^{2+}/CaM can interact with the $Na_V1.5$ CT using both its lobes. Our Ca^{2+}/CaM:CT structure only extends until $Na_V1.5$ residue 1922, since longer constructs failed to crystallize. However, ITC experiments show a clear increase in affinity of Ca^{2+}/CaM for the $Na_V1.5$ CT with progressively longer constructs. We previously observed a K_d of ∼2 μM for a $Na_V1.5$ CT construct ending at residue 1924 (16), but the K_d is ∼1 μM for a construct ending at residue 1927, and as low as 260 nM when ending at residue 1934 (Fig. 4 and *SI Appendix*, Table S2). Extending the construct beyond this did not result in any increase in affinity.

To gain further structural insights, we directly compared the binding sites for Ca^{2+}/C-lobe (our structure, PDB ID code 6MUD) and Ca^{2+}/N-lobe (mixed CaM complex, PDB ID code 4JQ0), to see whether combining both could represent the full Ca^{2+}/CaM complex. However, it is clear that such a mode cannot exist without some rearrangements, since the C terminus of the N-lobe and the N terminus of the C-lobe are more than 16 Å apart, too far to be connected by a single peptide bond (Fig. 4*D*).

Since the affinity of Ca^{2+}/CaM for the $Na_V1.5$ CT increases between residues 1924 and 1927 and beyond, we assumed that the additional binding determinants would reside in this area.

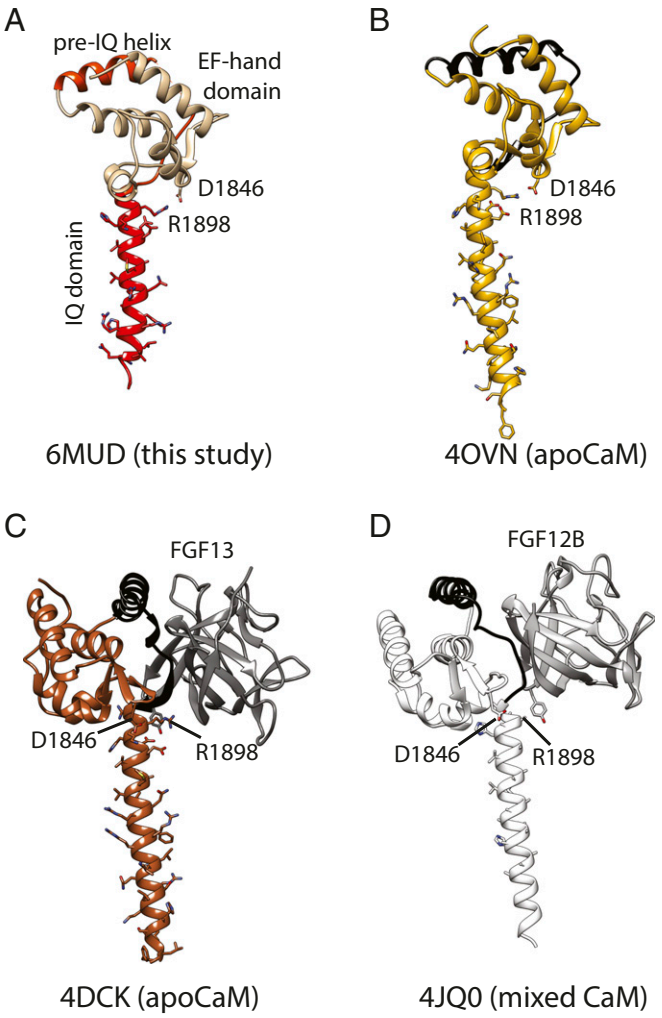

Fig. 3. FHF proteins dictate the relative conformation of EF-hand domain and IQ domain. Side-by-side comparison of four different Na_V CT structures, showing the same view based on superposition of the sixth helix containing the IQ domain. This highlights the relative orientation of EF-hand domain. CaM has been omitted from each structure for clarity. (*A*) Ca^{2+}/CaM complex without FHF (PDB ID code 6MUD, this study). (*B*) Ca^{2+} free, Mg^{2+} loaded CaM complex without FHF (PDB ID code 4OVN). (*C*) Ca^{2+}-free, Mg^{2+}-loaded CaM complex with FGF13 bound (PDB ID code 4DCK). (*D*) Mixed CaM complex with FGF12B bound (PDB ID code 4JQ0). The orientation of the EF-hand domain relative to the IQ domain is dictated by the presence or absence of FHF, and not by Ca^{2+} concentration. The two residues implicated in a salt bridge in the absence of FHFs, Asp1846 and Arg1898, are indicated. Binding of FHF breaks this salt bridge.

We noticed a hydrophobic cluster with sequence "FLF" formed by residues 1926–1928. Since Ca^{2+}/CaM often associates to targets via hydrophobic clusters, we mutated this region to AAA in a longer construct extending until residue 1934 and assessed the affinity. This results in a K_d of ∼5 μM (Fig. 4 and *SI Appendix*, Table S2), bringing it back to the affinity for the shorter constructs. We therefore conclude that these residues are part of the additional interaction site for the Ca^{2+}/N-lobe.

Differences Between Ca^{2+}/CaM Binding to $Ca_V1.2$ and $Na_V1.5$. Previously, several crystal structures have captured Ca^{2+}/CaM bound to the $Ca_V1.1$ and 1.2 IQ domain (28, 29, 31). These show substantial differences in binding mode compared with $Na_V1.5$. In the Ca_V complex, both lobes contribute to the binding, with the N-lobe located at the N-terminal portion of the IQ domain.

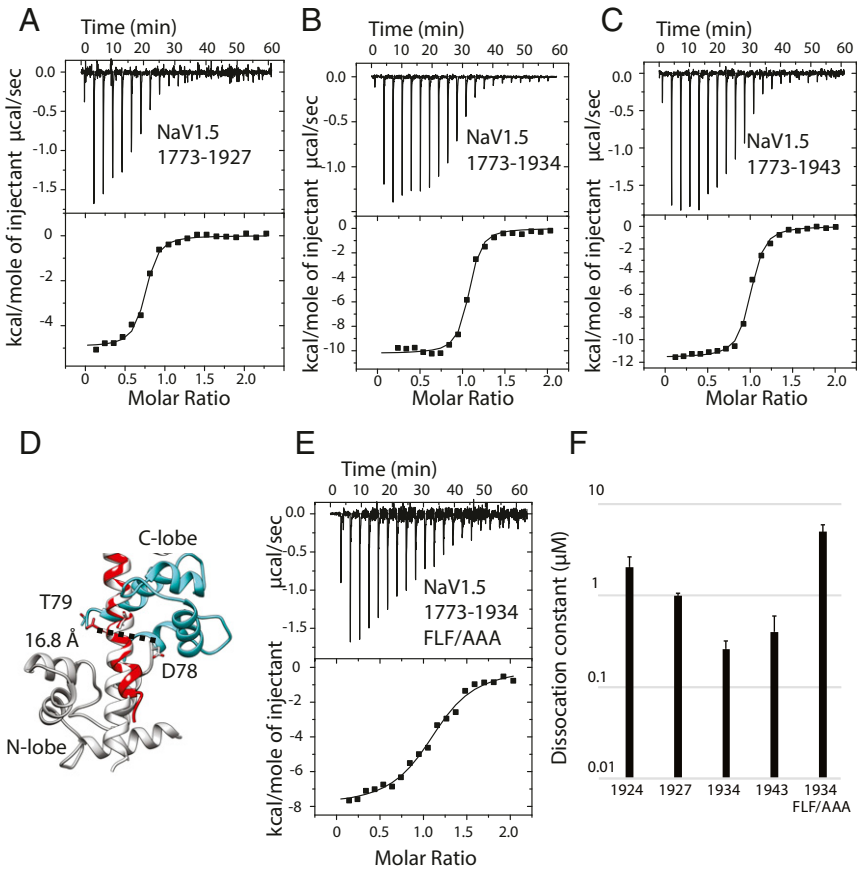

Fig. 4. Analysis of additional binding determinants downstream of the IQ domain. All titrations shown are in saturating Ca^{2+} conditions. (*A*) ITC measurement of 120 µM $Na_v1.5_{1773–1927}$ titrated with 1.2 mM CaM. K_d = 1.02 ± 0.07 µM. (*B*) ITC measurement of 50 µM $Na_v1.5_{1773–1934}$ titrated with 0.5 mM CaM. K_d = 0.26 ± 0.06 µM. (*C*) ITC measurement of 60 µM $Na_v1.5_{1773–1943}$ titrated with 0.6 mM CaM. K_d = 0.4 ± 0.2 µM. (*D*) Superposition based on the sixth helix containing the IQ domain to test a hypothetical combination of Ca^{2+}/C-lobe position (this study, blue) and Ca^{2+}/*N*-lobe (PDB ID code 4jq0, gray). The shown combination would lead to a clash around D78 and substantial distortion would have to occur to allow linking residues 78 and 79. (*E*) ITC measurement of 100 µM $Na_v1.5_{1773–1934}$ FLF1926AAA titrated with 1 mM CaM. K_d = 5 ± 1 µM. The mutation reduces binding affinity. (*F*) Bar graph showing K_d values for various constructs on a logarithmic scale. The numbers below each bar represent the residue number of the C terminus of each construct. The value for the construct ending at 1924 was taken from Sarhan et al. (16).

The binding affinity here is also much higher, with a K_d in the low nanomolar range for the Ca^{2+}/C-lobe alone (28, 40), and subpM for full Ca^{2+}/CaM (41). As the Ca^{2+}/C-lobe binding affinity for the $Na_V1.5$ CT is three orders of magnitude lower, substantial differences at the interface with the IQ domain are expected. Indeed, the $Ca_V1.2$ IQ domain contributes three aromatic residues to the interface with the Ca^{2+}/Clobe, whereas the $Na_V1.5$ IQ domain contributes none (*SI Appendix*, Fig. S4). There is also a ∼90° rotation of the Ca^{2+}/C-lobe relative to the IQ domain.

Disease Mutations in the $Na_V1.5$ IQ Domain Can Affect Either Ca^{2+}/CaM or apoCaM Binding. $Na_V1.5$ is the target for disease mutations linked to inherited arrhythmias, and four of these are located within the IQ domain, where they could interfere with either apoCaM and/or Ca^{2+}/CaM binding. Fig. 5 highlights the mutations, which were previously shown to be involved in apoCaM binding (33). E1901Q is at the N-terminal end of the IQ domain and has been involved in type-3 long-QT syndrome (LQT3) (42). It was shown to cause an increase in late sodium current up to 2.5% (43). However, this could be restored by increasing CaM expression. A Ca^{2+} dependence of the steady-state inactivation curve has not been investigated. Glu1901 is involved in a salt bridge with Lys95 in the apoCaM complex but not in any interactions with Ca^{2+}/CaM, as it is pointing to the solvent (Fig. 5 and *SI Appendix*, Fig. S5). Therefore, no effect is expected on Ca^{2+}/CaM binding.

Two additional mutations, Q1909R (LQT3) (44) and R1913H (LQT3) (42), are also at interfaces with apoCaM, but not with Ca^{2+}/CaM (Fig. 5 and *SI Appendix*, Fig. S5). Both were previously shown to cause an increase in late sodium current, and coexpression of excess CaM restores this to wild-type levels (43). No inherent shift in steady-state inactivation (SSI) was observed. A separate report confirmed that Q1909R causes an increase in late current, which could be normalized by increased cytosolic Ca^{2+} (45). It thus seems that, for mutations that affect apoCaM, but not Ca^{2+}/CaM binding, late currents could still be dampened by either adding excess CaM (which would compensate for a decreased affinity) or by adding Ca^{2+}, allowing the binding of Ca^{2+}/CaM. In the structure of the $Ca_V1.2$ IQ domain:Ca^{2+}/CaM complex, the equivalent Gln residue, which defines Q in the IQ motif, is involved in direct interactions with Ca^{2+}/CaM (28, 29). To verify that that this residue is not involved in binding the Ca^{2+}/C-lobe, we performed ITC experiments on the Q1909R mutant (*SI Appendix*, Fig. S5 and Table S2), which show a very similar affinity (K_d 7 ± 2 µM versus 9 ± 1 µM for wild type), in agreement with the structure.

S1904L causes an increase in late sodium currents (46). No inherent shift in SSI was observed. Rescue experiments increasing cytosolic Ca^{2+} or CaM expression have not been performed for this mutant. In contrast to the above mutants, S1904L (LQT3) (47) is predicted to affect interactions with both apoCaM and

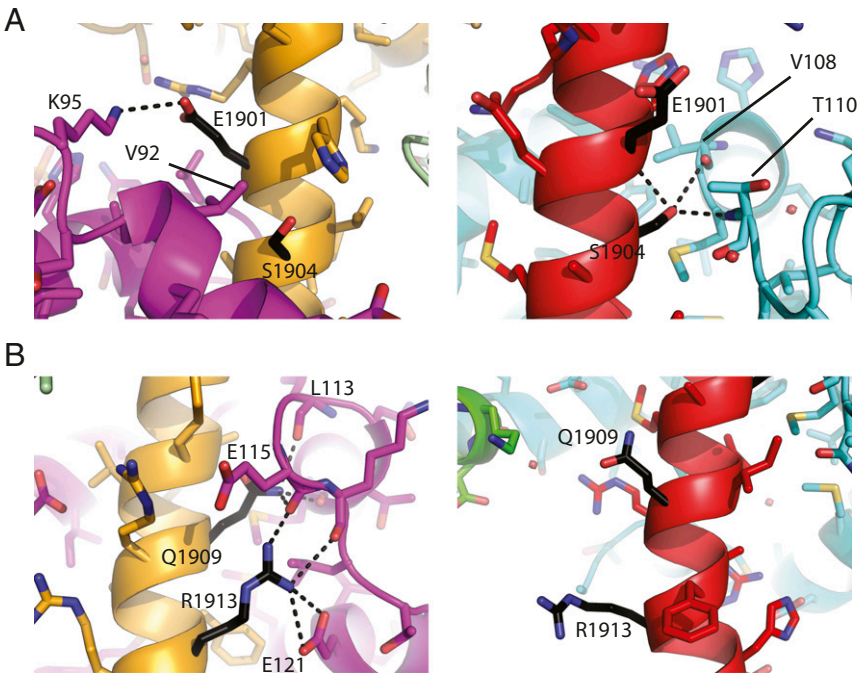

Fig. 5. Arrhythmia-associated mutations in the $Na_V1.5$ IQ domain. Side-by-side comparisons of positions of Long-QT mutations in the Ca^{2+}-free CaM (PDB 4OVN, *Left*) and Ca^{2+}/CaM complexes (PDB ID code 6MUD, current study, *Right*). Purple, Ca^{2+}-free C-lobe; green, Ca^{2+}/N-lobe; cyan, Ca^{2+}/C-lobe. Hydrogen bonds are indicated via dotted lines. Positions for residues targeted by the E1901Q and S1904L mutations (*A*) and by the Q1909R and R1913H mutations (*B*). CaM residues involved in interactions with the wild-type residues are labeled. In the Ca^{2+}/CaM complex, only S1904 is directly involved in interactions with the C-lobe. The same mutation sites, in respect to the Ca^{2+}/C-lobe surface, are shown in *SI Appendix*, Fig. S5.

Ca^{2+}/CaM: Ser1904 forms van der Waals packing interactions with the apoC-lobe and it hydrogen bonds to the main chain of residues 109 and 110 in the Ca^{2+}/C-lobe (Fig. 5). As it is also tightly packed against the Ca^{2+}/C-lobe (*SI Appendix*, Fig. S5), adding a bulkier Leu residue is predicted to cause steric hindrance. To verify the impact of the S1904L mutation on Ca^{2+}/CaM, we performed ITC experiments (*SI Appendix*, Fig. S5). As expected, the mutation has a significant impact on the affinity, yielding an isotherm that could not be fitted. In conclusion, the S1904L mutant is unique among these four, as it affects both apoCaM and Ca^{2+}/CaM binding.

Isoform-Specific Differences Between $Na_V1.4$ and $Na_V1.5$ Hint at a Mechanism for CDI. Ca^{2+}-uncaging experiments have shown that $Na_V1.4$ currents display a Ca^{2+}-sensitive inhibition, similar to CDI in Ca_V channels (21). $Na_V1.5$, although a close homolog, did not show this modulation. We therefore set out to characterize the interaction between Ca^{2+}/CaM and $Na_V1.4$. We noticed the absence of the "FLF" sequence, which increases the affinity for Ca^{2+}/CaM in $Na_V1.5$. Instead, this sequence is replaced by "YMY." To check whether $Na_V1.4$ has additional binding determinants for Ca^{2+}/CaM in this region, we compared peptides spanning $rNa_V1.4$ 1716–1744 or $rNa_V1.4$ 1716–1753, respectively. The obtained K_d values (*SI Appendix*, Table S2) were comparable between long and short IQ domain. This is in direct contrast with $Na_V1.5$, which contains an extra binding determinant.

We determined a structure of the $Na_V1.4$ IQ domain ($rNa_V1.4$ 1716–1744) in complex with Ca^{2+}/CaM. Fig. 6 shows how the interactions are driven by the C-lobe, with no contributions from the N-lobe. Interactions of note include salt bridges between $Na_V1.4$ residues Arg1729 and Arg1733 with the Ca^{2+}/C-lobe. Additional hydrogen bonds are formed by His1734 and Lys1726. Hydrophobic contacts are mostly contributed by Val1722 and Ile1725. Similar to $Na_V1.5$, no bulky hydrophobic Na_V residue occupies the deep hydrophobic pocket in the Ca^{2+}/C-lobe. Of note, a single Cys residue in the IQ domain is at a crystal contact with a neighboring molecule in the asymmetric unit. Although modeling a disulfide bond yields negative density, the possibility exists for Cys-mediated cross-linking, which would affect the binding mode of CaM. As many channels have displayed redox sensitivity through cysteine modifications, it will be of interest to see whether this applies to cysteine residues in the IQ domain.

A superposition with the $Na_V1.5$ CT:Ca^{2+}/CaM structure shows that the Ca^{2+}/C-lobe binding site is very different, engaging another set of IQ domain residues (Fig. 7*A*). Although the IQ domains are highly conserved, there are four differences in the sequence, three of which are directly involved in interactions (Fig. 6*E*). Ser1904 in $Na_V1.5$ makes two hydrogen bonds with the main chain of the Ca^{2+}/C-lobe, but in $Na_V1.4$ this is replaced with a Cys, which cannot make such H-bonds. $Na_V1.5$ residue Met1906, which makes van der Waals interactions with the Ca^{2+}/C-lobe, is replaced by Ile, which makes different van der Waals interactions. Val1907 in $Na_V1.5$ does not form any interactions but is replaced by Lys in $Na_V1.4$, whose side chain forms a hydrogen bond with the Ca^{2+}/C-lobe.

Because the Ca^{2+}/C-lobe occupies a different site on the IQ domain in $Na_V1.4$, we wondered whether it would be compatible with the position of the EF-hand domain. The salt bridge residues, which determine the relative orientation of EF-hand to IQ domain, are conserved in $Na_V1.4$, so the relative position, in the absence of CaM, is likely the same as in $Na_V1.5$. Fig. 7 *B* and *C* show that there would be a clash between the Ca^{2+}/C-lobe and the EF-hand domain in $Na_V1.4$ in such an orientation. Therefore, for Ca^{2+}/CaM to bind to its preferred site on the $Na_V1.4$ IQ domain, the EF-hand domain has to be at a different position compared with $Na_V1.5$. Potentially, such a movement of the EF-hand domain relative to the IQ domain, induced by binding of Ca^{2+} to CaM, may represent an allosteric switch through which Ca^{2+} binding results in CDI in $Na_V1.4$ (21).

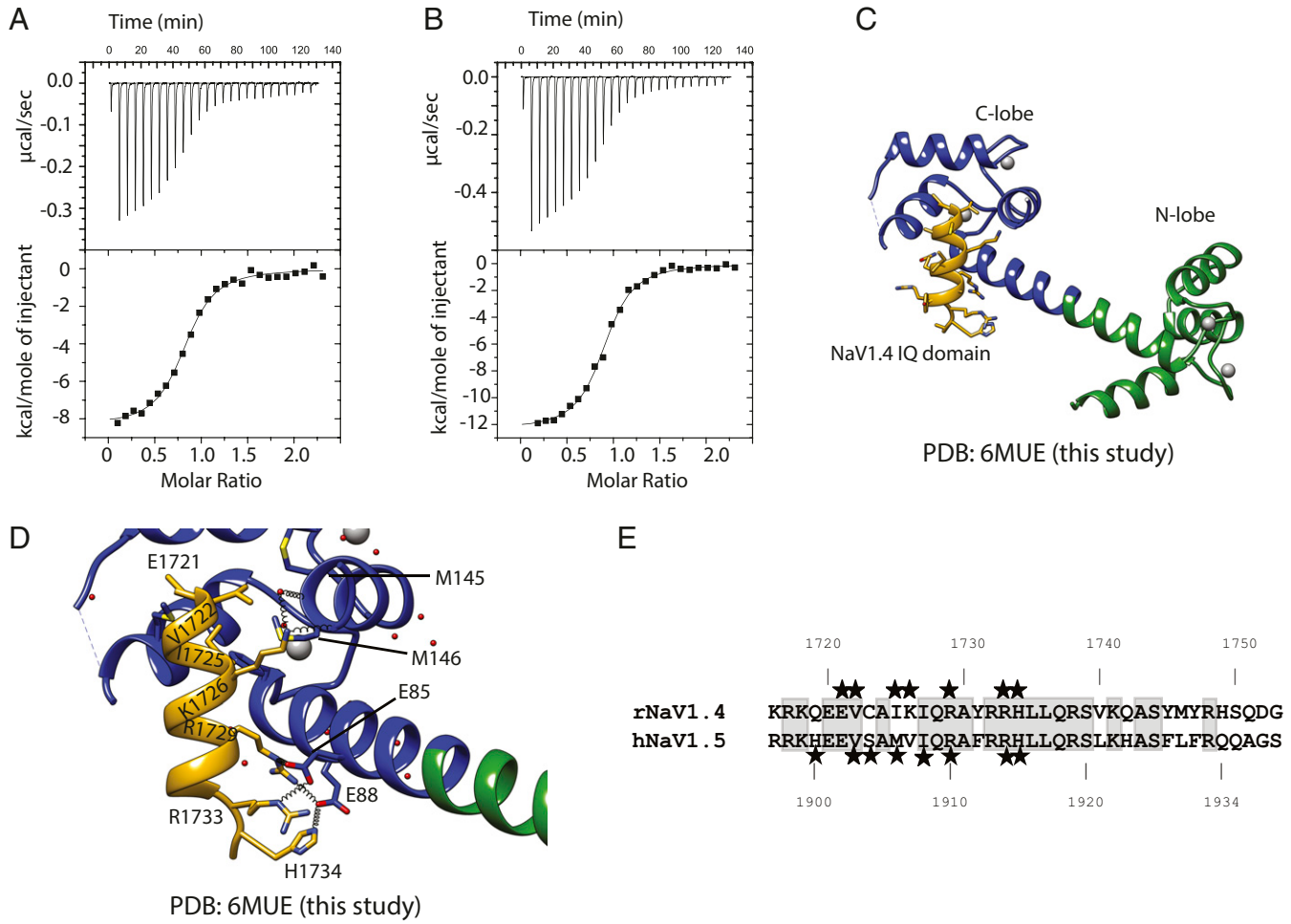

Fig. 6. Interactions of $Na_v1.4$ IQ domain with Ca^{2+}/CaM. (*A*) ITC measurement of $Na_v1.4_{1716–1744}$ titrated with Ca^{2+}/CaM. $K_d = 0.3 \pm 0.04$ µM. (*B*) ITC measurement of $Na_v1.4_{1716–1753}$ titrated with Ca^{2+}/CaM. $K_d = 0.27 \pm 0.02$ µM. (*C*) Crystal structure of $Na_v1.4_{1716–1744}$ in complex with Ca^{2+}/CaM. All binding is mediated by the C-lobe. (*D*) Details of interaction, hydrogen bonds, and a salt bridge network are indicated with distances. (*E*) Sequence alignment of $Na_v1.5$ and $rNa_v1.4$ CT region after the EF-hand domain. Asterisks indicate residues involved in interactions with Ca^{2+}/CaM. Conserved residues are shaded gray.

We therefore note several differences between $Na_V1.4$ and $Na_V1.5$ in regard to Ca^{2+}/CaM association: (*i*) a higher affinity for the IQ domain of $Na_V1.4$, (*ii*) the presence of a downstream binding determinant that increases the affinity for Ca^{2+}/CaM in $Na_V1.5$, and (*iii*) the Ca^{2+}/C-lobe engages different residues in the IQ domain, which may affect the relative position of the EF-hand and IQ domains in $Na_V1.4$.

Discussion

Ca_V and Na_V channels have adopted CaM as a resident Ca^{2+} sensor. Many Ca_V channels display CDI, a phenomenon that requires an EF-hand–like domain, as well as an IQ domain capable of binding CaM in both high and low Ca^{2+}. Although the EF-hand domain was shown to be crucial in this process (38), the exact conformational coupling from Ca^{2+} binding to channel inactivation has thus far remained a mystery. Structures thus far have failed to reveal a full mechanism, as any Ca_V construct containing both EF-hand–like domain and IQ domain has failed to crystallize, and cryo-EM studies of $Ca_V1.1$ have not revealed any density for the IQ domain (48).

Similarly, cryo-EM studies of Na_V channels have failed to reveal the IQ domain and until now no structure of a fully Ca^{2+}-occupied CaM bound to the CT of any Na_V had been resolved. Here we present a structure of a fully Ca^{2+}-occupied CaM bound to the CT of $Na_V1.5$. It is clear that a structure, previously interpreted as a fully Ca^{2+}-occupied CaM (13), represents a mixed CaM, whereby the C-lobe displays both the conformation and binding site of the apoC-lobe (Fig. 2).

What is the exact role of the Na_V EF-hand domain? Our results suggest that the precise orientation of this domain relative to the IQ domain may dictate the ability of Ca^{2+}/CaM to bind to the IQ domain. In both our structure and one previous structure of apoCaM bound to the $Na_V1.5$ CT, the EF-hand domain orientation relative to the IQ domain is identical, dictated in part by a salt bridge between Asp1846, located in the EF-hand domain, and Arg1898, at the N-terminal end of the IQ domain. Both residues are conserved in all nine human isoforms, with the exception of $Na_V1.8$, suggesting that other isoforms can form similar EF-hand to IQ orientations. The precise conformation of the EF-hand to the IQ domain may underlie disease. In $Na_V1.2$, for example, the R1902C mutation has been linked to familial autism (49). This residue is the equivalent of Arg1898 in NaV1.5, involved in the salt bridge with Asp1846. The disease mutation may thus affect conformation of the EF-hand domain relative to the IQ domain. Indeed, it was shown that the R1902C mutation caused a Ca^{2+}-dependent conformational switch in the $Na_V1.2$ CT, whereas wild type did not (50). It also was shown to induce a Ca^{2+}-dependent left shift in the steady-state inactivation (13).

This salt bridge can also be broken through binding of auxiliary proteins. FHF proteins, for example, sequester the Arg residue

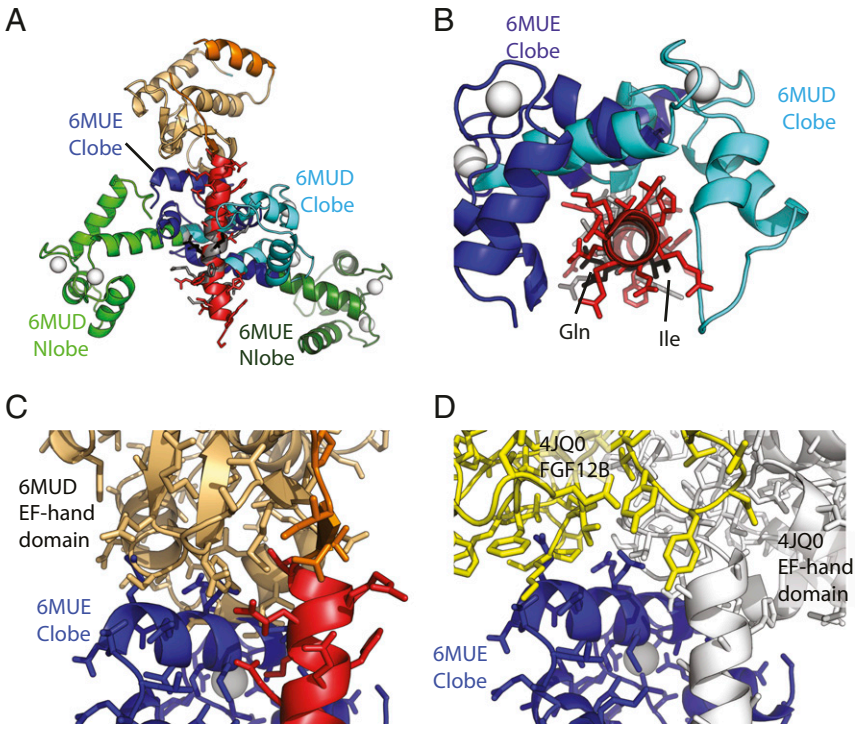

Fig. 7. Differences in IQ motif binding between $Na_v1.5$ and $Na_v1.4$. The structures were superposed based on Na_V CT helix 6, containing the IQ domain. (*A*) Superposition of the complexes $Na_V1.5$ CT:Ca^{2+}/CaM (PDB ID code 6MUD, this study) and $Na_V1.4$ IQ domain:Ca^{2+}/CaM (PDB ID code 6MUE, this study). N-lobe and C-lobe are shown in green and blue, respectively, with light colors for the $Na_V1.5$ complex and dark colors for the $Na_V1.4$ complex. $Na_V1.5$ EF-hand domain (beige), $Na_V1.5$ IQ domain (red), and $Na_V1.4$ IQ domain (gray) are shown. Calcium ions are shown as white spheres. (*B*) Same superposition as in *A* but with the view from the N terminus of the IQ domain toward the C terminus. The EF-hand domain has been omitted and only the C-lobes are shown. This indicates a ∼90° rotation of the C-lobe binding to $Na_V1.4$ compared with the $Na_V1.5$ IQ domain. The Ile and Gln residues of the "IQ" motif are shown in black for reference. (*C*) Same superposition as in *A*, but only showing the $Na_V1.5$ CT (EF-hand domain in beige; IQ domain in red) and the C-lobe from the $Na_V1.4$ complex. This shows that the C-lobe would clash with the EF-hand domain, suggesting that, for it to bind in this mode, the EF-hand domain in $Na_V1.4$ would have to be displaced. (*D*) Superposition, based on helix 6, for the $Na_V1.5$ CT: mixed-CaM complex with FGF12B (PDB ID code 4JQ0) and for the $Na_V1.4$ IQ: Ca^{2+}/CaM complex (PDB ID code 6MUE, this study). Shown are the $Na_V1.5$ CT (white) and FGF12B (yellow) from 4JQ0, and the C-lobe from the $Na_V1.4$ complex. This shows that, also in the presence of an FHF, there would be clashes between the Ca^{2+}/C-lobe and the EF-hand domain. In addition, clashes would occur between Ca^{2+}/Clobe and FGF12B.

involved in the salt bridge, resulting in a ∼180° reorientation of the EF-hand domain relative to the IQ domain (Fig. 3) (13, 25), thus preventing the Ca^{2+}/C-lobe from binding to the site we observe in this study (PDB ID code 6MUD).

How do Na_V isoforms differ in their ability to bind Ca^{2+}/CaM? A previous NMR structure was solved for the $Na_V1.2$ IQ domain in complex with the individual Ca^{2+}/C-lobe (36). Interestingly, the binding site here is different from the one in our $Na_V1.5$ CT structure (*SI Appendix*, Figs. S6 and S7). Similarly, we also solved a crystal structure of the $Na_V1.4$ IQ domain in complex with Ca^{2+}/CaM. The binding site for the Ca^{2+}/C-lobe differs from both the $Na_V1.2$ and $Na_V1.5$ binding sites, indicating that small substitutions in the IQ domain can result in different binding sites. The divergence between the isoforms is, however, expected, given the differences in affinities and function. For example, Ca^{2+}/CaM has been found to bind the $Na_V1.2$ IQ domain with a K_d ∼85 nM, roughly 25-fold stronger than to the $Na_V1.5$ IQ domain (K_d ∼2 μM) (16). Of note, the relatively weak affinity of Ca^{2+}/CaM for the $Na_V1.5$ CT may suggest that a proportion of the channels is not bound to CaM under elevated Ca^{2+} conditions, unless it is bridged to other segments such as the III–IV linker (16, 27).

Using Ca^{2+}-uncaging experiments, it was shown that $Na_V1.4$, an isoform expressed in skeletal muscle, displays a CDI-like behavior reminiscent of Ca_V channels (21). However, $Na_V1.5$ did not display this phenomenon, despite the high degree of sequence conservation in the CT region of both channels. Swapping the CTs between both channels showed that this region is responsible for the isoform-specific effect (21). We therefore set out to understand the intrinsic differences between $Na_V1.4$ and $Na_V1.5$.

Through a crystal structure of the isolated $Na_V1.4$ IQ domain in complex with Ca^{2+}/CaM, we noted that its binding mode would be incompatible with the position of the EF-hand domain as observed for $Na_V1.5$. One possibility is that the $Na_V1.4$ EF-hand domain forces Ca^{2+}/CaM to bind at a different position from the one we observe here or, alternatively, that the EF-hand domain adopts a different position when Ca^{2+}/CaM is bound (Fig. 8*A*). The situation is different in $Na_V1.5$, where both apoCaM and Ca^{2+}/CaM can bind to the IQ domain without steric clashes with the EF-hand domain, as long as FHFs are absent. As a result, Ca^{2+} binding to CaM would not produce a conformational rearrangement in $Na_V1.5$, explaining the absence of CDI for this channel (Fig. 8*B*). Interestingly, FHFs have been shown to abolish CDI in $Na_V1.4$ (26), an effect that may be ascribed to its inherent effect on the EF-hand orientation, locking it into a position such that no Ca^{2+}-dependent conformational change occurs. Similarly, STAC proteins, which can bind to two different regions in Ca_V1 channels (26, 51–56), including the EF-hand domain (26), could affect the relative orientation between EF-hand and IQ domain. How this conformational change further results in inactivation remains to be shown, but of note is the ability of the EF-hand domain to interact with the III–IV linker, and that this interaction affects channel inactivation (14). Future

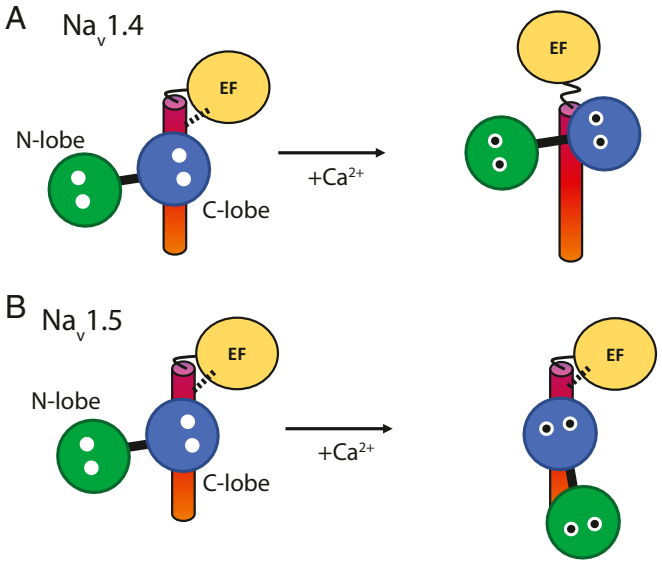

Fig. 8. Potential conformational switch mechanism for CDI. (*A*) $Na_V1.4$. Under Ca^{2+}-free conditions, CaM can bind to the IQ domain without disturbing the orientation of EF-hand domain to the IQ domain (salt bridge indicated by dotted line). Upon binding Ca^{2+}, the Ca^{2+}/C-lobe switches to a different site and dislodges the EF-hand domain. As the EF-hand domain can also bind to the III–IV linker, an interaction that modulates inactivation (14), this could then affect inactivation. (*B*) $Na_V1.5$. Under both Ca^{2+}-free and Ca^{2+}-loaded conditions, CaM can bind to the IQ domain without disturbing the EF-hand domain. Therefore, no conformational change occurs that could be linked to CDI.

structures with longer $Na_V1.4$ fragments will be of use to check the results here obtained with a short peptide.

The above hypothesis remains to be proven, but another inherent difference between the CT regions of $Na_V1.4$ and $Na_V1.5$ should be considered. For $Na_V1.5$, we found that a hydrophobic "FLF" cluster, formed by residues 1926–1928, results in an increase in affinity for Ca^{2+}/CaM. In $Na_V1.4$, however, there is no increase in affinity by extending the construct (*SI Appendix*, Table S2), either due to the different identity of the residues here, or because the different Ca^{2+}/C-lobe position may not be sterically compatible with binding of the Ca^{2+}/N-lobe in this area. The functional relevance of this observation is that this gives more freedom for the Ca^{2+}/N-lobe to bind elsewhere in $Na_V1.4$, exerting effects not happening for $Na_V1.5$.

We conclude that the EF-hand domain in Na_Vs plays a key role in dictating the binding mode of CaM to the IQ domain and may mediate the Ca^{2+}-dependent conformational switch that underlies CDI. In the case of a bound FHF, the implication is that this induces a stable interface between FHF, EF-hand domain, and IQ domain, such that Ca^{2+}/CaM cannot knock off the bound FHF. In such a case, the FHF dictates the binding mode of CaM through the use of the EF-hand domain. In the absence of an FHF, however, the interaction between EF-hand domain and IQ domain is relatively weak, such that binding of Ca^{2+}/CaM can displace the EF-hand domain.

Given the similarities between Na_V and Ca_V channels in regard to CDI (21), similar mechanisms may exist for several isoforms of Ca_Vs, whereby the position of the EF-hand domain regulates CDI. Interestingly, STAC proteins have recently been found to engage Ca_Vs (51–57) and were shown to interact with the EF-hand domain, abolishing CDI (26). This is reminiscent of the effect of FHFs on Na_Vs, and it was shown that FHFs can abolish CDI in $Na_V1.4$ (26). Although there are parallels between Na_V and Ca_V channels in regard to CaM regulation, there is also divergence. For example, Na_V CT fragments bind Ca^{2+}-free CaM stronger than Ca^{2+}/CaM, opposite to most Ca_V1 and Ca_V2 channels. CaM has also been reported to interact with the III–IV linker in $Na_V1.5$ (16, 27), but so far this has not yet been described for Ca_Vs.

Finally, CaM is targeted by mutations linked to inherited arrhythmias (58, 59), and several of these have been shown to alter the binding mode of Ca^{2+}/CaM or apoCaM with the $Ca_V1.2$ IQ domain (40). As some of these have been shown to affect $Na_V1.5$ function (4, 60), it will be interesting to test whether any of these also alter the binding mode to Na_V channels, and whether the EF-hand domain plays a role in this.

During review of this manuscript, a paper was published describing complexes of apoCaM and Ca^{2+}/CaM with the $Na_{1.4}$ CT, containing both the EF-hand domain and IQ domain (61). The authors found both the apoC-lobe and Ca^{2+}/C-lobe to bind to a site nearly identical to the previously identified apoC-lobe binding site in $Na_V1.5$. This site is different from the Ca^{2+}/C-lobe binding site in the $Na_V1.4$ IQ complex we described in this study (PDB ID code 6MUE) showing that, also in the case of $Na_V1.4$, the EF-hand domain can affect the binding mode of Ca^{2+}/CaM through steric hindrance. Whether the Ca^{2+}/C-lobe can displace the $Na_V1.4$ EF-hand under physiological conditions remains to be shown.

Methods

Protein Production. All $Na_V1.5$ constructs were expressed in a modified pET28 vector containing a maltose binding protein tag and a His-tag. A clone for human CaM was previously generated (28). All proteins were expressed in *Escherichia coli* Rosetta (DE3) pLacI cells grown in 2YT media and induced with 0.4 mM isopropyl β-D-1-thiogalactopyranoside and purified using chromatography with nickel and amylose affinity columns, followed by ion exchange and size exclusion columns. Additional details are shown in *SI Appendix, Supplementary Methods*.

Crystallization and Structure Solution. The construct $Na_V1.5_{1786–1922}$ was coexpressed with CaM in *E. coli Rosetta DE3 pLacI* cells using the same procedure as described before (28). Before crystallization, the protein was concentrated to 6 mg·mL^{-1} using Amicon concentrators (10-kDa molecular weight cutoff; Millipore). All crystals were obtained using the hanging-drop method at 4 °C. $Na_V1.5$ and CaM were cocrystallized in 5 to 15% (wt/vol) PEG 4000, 0.1 M Tris, pH 9.5, 0.1 M $MgCl_2$, and 5% (vol/vol) isopropanol. All crystals were flash-frozen in liquid N_2 in the corresponding mother liquor containing an additional 25 to 30% (wt/vol) sucrose.

For the $Na_V1.4$ IQ domain:Ca^{2+}/CaM complex, synthetic peptide was mixed with purified CaM at a 1:1 ratio. Crystallization was achieved in hanging-drop plates with 0.1 M MES pH 6.0 and 55% (vol/vol) isopropanol. Crystals were flash-frozen in liquid N_2 without further addition of cryoprotectant.

Data for the $Na_V1.5$ CT:Ca^{2+}/CaM complex were collected at beamline 23ID-D of the Advanced Photon Source (APS), and data for the $Na_V1.4$ IQ:Ca^{2+}/CaM complex were collected at APS beamline 23ID-B. Data were processed with XDS (62), phases obtained through molecular replacement using Phaser, and the structures refined using REFMAC 5.8.0071 (63) and Coot (64). Statistics are shown in *SI Appendix*, Table S1. The final structures have been deposited in the PDB database with accession numbers 6MUD (65) and 6MUE (66). Additional details are shown in *SI Appendix, Supplementary Methods*.

ITC. The experiments for the various $Na_V1.5$ CT constructs were performed using an ITC200 instrument (MicroCal), while the experiments with $Na_V1.4$ IQ-only peptides were run with a VP-ITC instrument (MicroCal). The binding isotherms were analyzed using a single-site binding model with the vendor-supplied modified version of Origin 7.0 (OriginLab). Additional details are shown in *SI Appendix, Supplementary Methods*.

ACKNOWLEDGMENTS. We thank Omid Haji-Ghassemi for assistance with ITC data analysis and the support staff at the Advanced Photon Source (Chicago) GM/CA-CAT beamline 23-ID-D, the Stanford Synchrotron Radiation Lightsource (Menlo Park), and the Canadian Light Source (Saskatoon, SK, Canada), which is supported by the Natural Sciences and Engineering Research Council of Canada, the National Research Council Canada, the Canadian Institutes of Health Research (CIHR), the Province of Saskatchewan, Western Economic Diversification Canada, and the University of Saskatchewan. This work was supported by CIHR Grant MOP-119404 (to F.V.P.).

1. Ahern CA, Payandeh J, Bosmans F, Chanda B (2016) The hitchhiker's guide to the voltage-gated sodium channel galaxy. *J Gen Physiol* 147:1–24.
2. Winters JJ, Isom LL (2016) Developmental and regulatory functions of Na(+) channel non-pore-forming β subunits. *Curr Top Membr* 78:315–351.
3. Yan Z, et al. (2017) Structure of the Nav1.4-beta1 complex from electric eel. *Cell* 170: 470–482.e11.
4. Yin G, et al. (2014) Arrhythmogenic calmodulin mutations disrupt intracellular cardiomyocyte Ca2+ regulation by distinct mechanisms. *J Am Heart Assoc* 3:e000996.
5. Shen H, et al. (2017) Structure of a eukaryotic voltage-gated sodium channel at near-atomic resolution. *Science* 355:eaal4326.
6. Das S, Gilchrist J, Bosmans F, Van Petegem F (2016) Binary architecture of the Nav1.2-β2 signaling complex. *eLife* 5:e10960.
7. Gilchrist J, Das S, Van Petegem F, Bosmans F (2013) Crystallographic insights into sodium-channel modulation by the β4 subunit. *Proc Natl Acad Sci USA* 110:E5016–E5024.
8. Namadurai S, et al. (2014) Crystal structure and molecular imaging of the Nav channel β3 subunit indicates a trimeric assembly. *J Biol Chem* 289:10797–10811.
9. Shimizu H, et al. (2016) Structure-based site-directed photo-crosslinking analyses of multimeric cell-adhesive interactions of voltage-gated sodium channel β subunits. *Sci Rep* 6:26618.
10. Miloushev VZ, et al. (2009) Solution structure of the NaV1.2 C-terminal EF-hand domain. *J Biol Chem* 284:6446–6454.
11. Chagot B, Potet F, Balser JR, Chazin WJ (2009) Solution NMR structure of the C-terminal EF-hand domain of human cardiac sodium channel NaV1.5. *J Biol Chem* 284:6436–6445.
12. Wingo TL, et al. (2004) An EF-hand in the sodium channel couples intracellular calcium to cardiac excitability. *Nat Struct Mol Biol* 11:219–225.
13. Wang C, et al. (2014) Structural analyses of Ca^{2+}/CaM interaction with NaV channel C-termini reveal mechanisms of calcium-dependent regulation. *Nat Commun* 5:4896.
14. Gardill BR, et al. (2018) The voltage-gated sodium channel EF-hands form an interaction with the III-IV linker that is disturbed by disease-causing mutations. *Sci Rep* 8:4483.
15. Van Petegem F, Lobo PA, Ahern CA (2012) Seeing the forest through the trees: Towards a unified view on physiological calcium regulation of voltage-gated sodium channels. *Biophys J* 103:2243–2251.
16. Sarhan MF, Tung CC, Van Petegem F, Ahern CA (2012) Crystallographic basis for calcium regulation of sodium channels. *Proc Natl Acad Sci USA* 109:3558–3563.
17. Sarhan MF, Van Petegem F, Ahern CA (2009) A double tyrosine motif in the cardiac sodium channel domain III-IV linker couples calcium-dependent calmodulin binding to inactivation gating. *J Biol Chem* 284:33265–33274.
18. Potet F, et al. (2009) Functional interactions between distinct sodium channel cytoplasmic domains through the action of calmodulin. *J Biol Chem* 284:8846–8854.
19. Biswas S, DiSilvestre D, Tian Y, Halperin VL, Tomaselli GF (2009) Calcium-mediated dual-mode regulation of cardiac sodium channel gating. *Circ Res* 104:870–878.
20. Tan HL, et al. (2002) A calcium sensor in the sodium channel modulates cardiac excitability. *Nature* 415:442–447.
21. Ben-Johny M, et al. (2014) Conservation of Ca2+/calmodulin regulation across Na and Ca2+ channels. *Cell* 157:1657–1670.
22. Zühlke RD, Pitt GS, Deisseroth K, Tsien RW, Reuter H (1999) Calmodulin supports both inactivation and facilitation of L-type calcium channels. *Nature* 399:159–162.
23. Ben-Johny M, Yue DT (2014) Calmodulin regulation (calmodulation) of voltage-gated calcium channels. *J Gen Physiol* 143:679–692.
24. Peterson BZ, DeMaria CD, Adelman JP, Yue DT (1999) Calmodulin is the Ca2+ sensor for Ca2+ -dependent inactivation of L-type calcium channels. *Neuron* 22:549–558.
25. Wang C, Chung BC, Yan H, Lee SY, Pitt GS (2012) Crystal structure of the ternary complex of a NaV C-terminal domain, a fibroblast growth factor homologous factor, and calmodulin. *Structure* 20:1167–1176.
26. Niu J, et al. (2018) Allosteric regulators selectively prevent Ca^{2+}-feedback of Ca_V and Na_V channels. *eLife* 7:e35222.
27. Johnson CN, et al. (2018) A mechanism of calmodulin modulation of the human cardiac sodium channel. *Structure* 26:683–694.e3.
28. Van Petegem F, Chatelain FC, Minor DL, Jr (2005) Insights into voltage-gated calcium channel regulation from the structure of the CaV1.2 IQ domain-Ca2+/calmodulin complex. *Nat Struct Mol Biol* 12:1108–1115.
29. Fallon JL, Halling DB, Hamilton SL, Quiocho FA (2005) Structure of calmodulin bound to the hydrophobic IQ domain of the cardiac Ca(v)1.2 calcium channel. *Structure* 13: 1881–1886.
30. Mori MX, Vander Kooi CW, Leahy DJ, Yue DT (2008) Crystal structure of the CaV2 IQ domain in complex with Ca2+/calmodulin: High-resolution mechanistic implications for channel regulation by Ca2+. *Structure* 16:607–620.
31. Halling DB, et al. (2009) Determinants in CaV1 channels that regulate the Ca2+ sensitivity of bound calmodulin. *J Biol Chem* 284:20041–20051.
32. Kim EY, et al. (2010) Multiple C-terminal tail Ca(2+)/CaMs regulate Ca(V)1.2 function but do not mediate channel dimerization. *EMBO J* 29:3924–3938.
33. Gabelli SB, et al. (2014) Regulation of the NaV1.5 cytoplasmic domain by calmodulin. *Nat Commun* 5:5126.
34. Isbell HM, Kilpatrick AM, Lin Z, Mahling R, Shea MA (2018) Backbone resonance assignments of complexes of apo human calmodulin bound to IQ motif peptides of voltage-dependent sodium channels $Na_V1.1$, $Na_V1.4$ and $Na_V1.7$. *Biomol NMR Assign* 12:283–289.
35. Feldkamp MD, Yu L, Shea MA (2011) Structural and energetic determinants of apo calmodulin binding to the IQ motif of the Na(V)1.2 voltage-dependent sodium channel. *Structure* 19:733–747.
36. Hovey L, et al. (2017) Calcium triggers reversal of calmodulin on nested anti-parallel sites in the IQ motif of the neuronal voltage-dependent sodium channel $Na_V1.2$. *Biophys Chem* 224:1–19.
37. Wilson MA, Brunger AT (2000) The 1.0 a crystal structure of Ca(2+)-bound calmodulin: An analysis of disorder and implications for functionally relevant plasticity. *J Mol Biol* 301:1237–1256.
38. Ben Johny M, Yang PS, Bazzazi H, Yue DT (2013) Dynamic switching of calmodulin interactions underlies Ca2+ regulation of CaV1.3 channels. *Nat Commun* 4:1717.
39. Houdusse A, et al. (2006) Crystal structure of apo-calmodulin bound to the first two IQ motifs of myosin V reveals essential recognition features. *Proc Natl Acad Sci USA* 103: 19326–19331.
40. Wang K, et al. (2018) Arrhythmia mutations in calmodulin cause conformational changes that affect interactions with the cardiac voltage-gated calcium channel. *Proc Natl Acad Sci USA* 115:E10556–E10565.
41. Findeisen F, Rumpf CH, Minor DL, Jr (2013) Apo states of calmodulin and CaBP1 control CaV1 voltage-gated calcium channel function through direct competition for the IQ domain. *J Mol Biol* 425:3217–3234.
42. Napolitano C, et al. (2005) Genetic testing in the long QT syndrome: Development and validation of an efficient approach to genotyping in clinical practice. *JAMA* 294: 2975–2980.
43. Yan H, Wang C, Marx SO, Pitt GS (2017) Calmodulin limits pathogenic Na+ channel persistent current. *J Gen Physiol* 149:277–293.
44. Tester DJ, Will ML, Haglund CM, Ackerman MJ (2005) Compendium of cardiac channel mutations in 541 consecutive unrelated patients referred for long QT syndrome genetic testing. *Heart Rhythm* 2:507–517.
45. Abdelsayed M, et al. (2017) Differential calcium sensitivity in Na_V 1.5 mixed syndrome mutants. *J Physiol* 595:6165–6186.
46. Glaaser IW, et al. (2012) Perturbation of sodium channel structure by an inherited long QT syndrome mutation. *Nat Commun* 3:706.
47. Bankston JR, et al. (2007) A novel LQT-3 mutation disrupts an inactivation gate complex with distinct rate-dependent phenotypic consequences. *Channels (Austin)* 1: 273–280.
48. Wu J, et al. (2016) Structure of the voltage-gated calcium channel Ca(v)1.1 at 3.6 Å resolution. *Nature* 537:191–196.
49. Weiss LA, et al. (2003) Sodium channels SCN1A, SCN2A and SCN3A in familial autism. *Mol Psychiatry* 8:186–194.
50. Kim J, et al. (2004) Calmodulin mediates Ca2+ sensitivity of sodium channels. *J Biol Chem* 279:45004–45012.
51. Campiglio M, Flucher BE (2017) STAC3 stably interacts through its C1 domain with $Ca_V1.1$ in skeletal muscle triads. *Sci Rep* 7:41003.
52. Wong King Yuen SM, Campiglio M, Tung CC, Flucher BE, Van Petegem F (2017) Structural insights into binding of STAC proteins to voltage-gated calcium channels. *Proc Natl Acad Sci USA* 114:E9520–E9528.
53. Campiglio M, et al. (2018) STAC proteins associate to the IQ domain of CaV1.2 and inhibit calcium-dependent inactivation. *Proc Natl Acad Sci USA* 115:1376–1381.
54. Polster A, Perni S, Bichraoui H, Beam KG (2015) Stac adaptor proteins regulate trafficking and function of muscle and neuronal L-type Ca2+ channels. *Proc Natl Acad Sci USA* 112:602–606.
55. Polster A, et al. (2018) Stac proteins suppress Ca^{2+}-dependent inactivation of neuronal l-type Ca^{2+} channels. *J Neurosci* 38:9215–9227.
56. Polster A, Nelson BR, Papadopoulos S, Olson EN, Beam KG (2018) Stac proteins associate with the critical domain for excitation-contraction coupling in the II-III loop of $Ca_V1.1$. *J Gen Physiol* 150:613–624.
57. Polster A, Nelson BR, Olson EN, Beam KG (2016) Stac3 has a direct role in skeletal muscle-type excitation-contraction coupling that is disrupted by a myopathy-causing mutation. *Proc Natl Acad Sci USA* 113:10986–10991.
58. Nyegaard M, et al. (2012) Mutations in calmodulin cause ventricular tachycardia and sudden cardiac death. *Am J Hum Genet* 91:703–712.
59. Crotti L, et al. (2013) Calmodulin mutations associated with recurrent cardiac arrest in infants. *Circulation* 127:1009–1017.
60. Boczek NJ, et al. (2016) Spectrum and prevalence of CALM1-, CALM2-, and CALM3-encoded calmodulin variants in long QT syndrome and functional characterization of a novel long QT syndrome-associated calmodulin missense variant, E141G. *Circ Cardiovasc Genet* 9:136–146.
61. Yoder JB, et al. (2019) Ca^{2+}-dependent regulation of sodium channels $Na_V1.4$ and $Na_V1.5$ is controlled by the post-IQ motif. *Nat Commun* 10:1514.
62. Kabsch W (2010) Xds. *Acta Crystallogr D Biol Crystallogr* 66:125–132.
63. Murshudov GN, et al. (2011) REFMAC5 for the refinement of macromolecular crystal structures. *Acta Crystallogr D Biol Crystallogr* 67:355–367.
64. Emsley P, Lohkamp B, Scott WG, Cowtan K (2010) Features and development of Coot. *Acta Crystallogr D Biol Crystallogr* 66:486–501.
65. Gardill BR, Tung CC, Van Petegem F (2018) Voltage-gated sodium channel $Na_V1.5$ C-terminal domain in complex with Ca^{2+}/calmodulin. Protein Data Bank. Available at https://www.rcsb.org/structure/6MUD. Deposited October 24, 2018.
66. Gardill BR, Tung CC, Van Petegem F (2018) Voltage-gated sodium channel $Na_V1.4$ IQ domain in complex with Ca^{2+}/calmodulin. Protein Data Bank. Available at https://www.rcsb.org/structure/6MUE. Deposited October 24, 2018.
67. Kyte J, Doolittle RF (1982) A simple method for displaying the hydropathic character of a protein. *J Mol Biol* 157:105–132.